








Layer-dependence of macroscopic and atomic magnetic correlations in Co/Pd multilayers

Cite as: AIP Advances **10**, 065321 (2020); <https://doi.org/10.1063/5.0010066>

Submitted: 06 April 2020 . Accepted: 02 June 2020 . Published Online: 18 June 2020

N. Soriano, B. Mora, V. Rollano, P. Gargiani, C. Quirós, F. Gálvez, C. Redondo, J. del Valle, I. Montoya, A. Gómez , E. M. González , E. Navarro , M. Vélez , J. M. Alameda, M. Valvidares , J. L. Vicent , and R. Morales 

COLLECTIONS

Paper published as part of the special topic on [Chemical Physics](#), [Energy, Fluids and Plasmas](#), [Materials Science](#) and [Mathematical Physics](#)



View Online



Export Citation



CrossMark

ARTICLES YOU MAY BE INTERESTED IN

[Introduction to antiferromagnetic magnons](#)

Journal of Applied Physics **126**, 151101 (2019); <https://doi.org/10.1063/1.5109132>

[Enhancement of perpendicular magnetic anisotropy of ferromagnet/oxide heterointerface by an oxygen-dependent orbital modulation](#)

Applied Physics Letters **116**, 022414 (2020); <https://doi.org/10.1063/1.5140606>

[Magnetic nanostructures for emerging biomedical applications](#)

Applied Physics Reviews **7**, 011310 (2020); <https://doi.org/10.1063/1.5121702>



NEW!

Sign up for topic alerts
New articles delivered to your inbox



Layer-dependence of macroscopic and atomic magnetic correlations in Co/Pd multilayers

Cite as: AIP Advances 10, 065321 (2020); doi: 10.1063/5.0010066

Submitted: 6 April 2020 • Accepted: 2 June 2020 •

Published Online: 18 June 2020



View Online



Export Citation



CrossMark

N. Soriano,¹ B. Mora,¹ V. Rollano,² P. Gargiani,³ C. Quirós,^{4,5} F. Gálvez,⁶ C. Redondo,¹ J. del Valle,^{6,a)} I. Montoya,¹ A. Gómez,^{6,b)}  E. M. González,^{2,6}  E. Navarro,⁶  M. Vélez,^{4,5}  J. M. Alameda,^{4,5} M. Valdares,³  J. L. Vicent,^{2,6}  and R. Morales^{7,8,c)} 

AFFILIATIONS

¹Department of Physical-Chemistry, University of the Basque Country UPV/EHU, 48940 Leioa, Spain

²IMDEA-Nanociencia, Faraday 8, Cantoblanco, 28049 Madrid, Spain

³ALBA Synchrotron Light Source, Cerdanyola del Valles, 08290 Barcelona, Spain

⁴Depto. Física, Fac. Ciencias, Universidad de Oviedo, Calle Federico García Lorca 18, 33007 Oviedo, Spain

⁵Centro de Investigación en Nanomateriales y Nanotecnología—CINN (CSIC—Univ. de Oviedo—Principado de Asturias), 33940 El Entrego, Spain

⁶Depto. Física Materiales, Facultad CC. Físicas, Universidad Complutense, 28040 Madrid, Spain

⁷Department of Physical-Chemistry and BCMaterials, University of the Basque Country UPV/EHU, 48940 Leioa, Spain

⁸IKERBASQUE, Basque Foundation for Science, 48011 Bilbao, Spain

^{a)} Present address: Department of Physics, University of California San Diego, CA 92093, USA.

^{b)} Present address: Centro de Astrobiología, INTA-CSIC, 28850 Torrejon de Ardoz, Spain.

^{c)} Author to whom correspondence should be addressed: rafael.morales@ehu.es

ABSTRACT

The development of multilayered materials with engineered magnetic properties compels a deep knowledge of physical properties at the atomic scale. The magnetic anisotropy is a key property in these materials. This work accounts for the magnetic anisotropy energy and its correlation with atomic properties of Co/Pd multilayers with the number of Co/Pd repetitions. Magnetometry measurements confirm stronger perpendicular magnetic anisotropy energies as the number of repetitions increases up to 40. However, the intrinsic anisotropy, related to the Co–Pd orbital hybridization and spin–orbit coupling, saturates at 15 repetitions. This finding is supported by x-ray magnetic circular dichroism analysis that reveals a direct correlation of the atomic Co and Pd orbital magnetic moments and the effective anisotropy of the system. The proximity effect that accounts for the Pd induced magnetization, along with the increasing Co moment, provides a suitable mechanism for the observed anisotropy energy layer dependence.

© 2020 Author(s). All article content, except where otherwise noted, is licensed under a Creative Commons Attribution (CC BY) license (<http://creativecommons.org/licenses/by/4.0/>). <https://doi.org/10.1063/5.0010066>

The magnetic anisotropy is one of the most important parameters in the technological applications of magnetic thin films. Materials with either high or low, in-plane (IP) or out of plane (OoP) anisotropy are required depending on specific applications.^{1–6} The control of the macroscopic properties conducting a microscopic control at the nanoscale is an essential goal of the materials science engineering, and crucial in new spintronic devices based on spin-orbit and spin-transfer torque.^{7–9} Co/Pd multilayers have widely

been studied for these applications due to their strong spin–orbit interactions and perpendicular magnetic anisotropy (PMA). It is known that the magnitude and direction of the magnetic anisotropy can be manipulated through the crystalline texture of the material, film thickness, and interfacial effects.^{10–16} Magnetic films of tens of nanometers in thickness usually present in-plane magnetization because of the shape anisotropy. On the contrary, as the magnetic layer becomes thinner, surface effects can dominate the

bulk properties of the film.^{17,18} The symmetry-breaking at the surface induces the so-called surface anisotropy perpendicular to the sample plane, therefore, competing with the shape anisotropy.^{19–25} Atoms near the surface or interface experience a reduced symmetry and different bonds than those in the bulk, which lead to a variety of magnetic phenomena such as out of plane anisotropy, enhancement of magnetic moments, and magnetic polarization of non-magnetic elements.^{26–30} A key factor for these phenomena is the spin-orbit interaction that couples spins to the electronic orbits of the crystal lattice. Hence, Co/Pd is an attractive system to study all these phenomena.

This work reports on the evolution of the magnetic anisotropy energy, the IP and OoP anisotropy, and its microscopic origin in Co/Pd multilayers as a function of the number of repetitions (n). Samples from $n = 2$ to 40 were deposited by sputtering, and structurally characterized by x-ray diffraction and transmission electron microscopy (TEM). Magnetic properties of the whole multilayer, as the saturation magnetization and the effective anisotropy, were obtained from the magnetization curves measured by the superconducting quantum interference device (SQUID) magnetometry. The atomic Co and Pd magnetic moments—spin and orbital components—and the anisotropy of the Co-orbital magnetic moment were evaluated from x-ray magnetic circular dichroism (XMCD) spectra. The results demonstrate that the PMA of Co/Pd multilayers can be tuned from very low values to a maximum magnitude with the number of repetitions. It was also found that the increase in the Co-orbital moment with n correlates with the intrinsic anisotropy of the Co/Pd interface. Such a moment increase is also reflected in a similar trend on the Pd moment induced by the proximity effect. These results provide insight into the underlying

physics at the atomic scale of the macroscopic properties of the Co/Pd multilayers.

Si//[Pd(0.6)/Co(0.4)] n /Pd(2.4) (thickness in nm) multilayers were grown at room temperature on a naturally oxidized Si (100) wafer by magnetron sputtering.^{31,32} The base pressure was 5×10^{-8} Torr, and the Ar sputtering pressure was 12 mTorr. Pd(0.6 nm)/Co(0.4 nm) bilayers were consecutively deposited n times and protected with a capping layer of Pd(2.4 nm). The number of repetitions, n , was varied from 2 to 40.

Cross-sectional TEM images of thicker samples (not shown) reveal the formation of grains with slightly different orientations. However, the Co/Pd crystals are not randomly oriented. X-ray high-angle diffraction θ - 2θ scans show a textured *fcc*-[111] orientation of grains.

Magnetization curves of Co/Pd multilayers were measured by SQUID for $n = 2, 5, 10, 15, 20,$ and 40. The hysteresis loops with the external field applied in the sample plane (IP) and perpendicular to the sample surface [out of plane (OoP)] are plotted in Fig. 1. The magnetic moment was normalized for comparison with the number of repetitions. Ultra-thin films ($n = 2$) do not show an easy anisotropy axis. Both IP and OoP curves overlap each other with a zero magnetization remanence and no coercivity. An easy anisotropy axis develops by increasing the number of Co/Pd repetitions. IP and OoP hysteresis loops differentiate for $n = 5$. The OoP signal becomes a square-slanted hysteresis loop with a finite coercive field ($H_C = 200$ Oe) and a normalized remanence $m_r = 0.33$. On the contrary, the IP magnetization curve is almost reversible, $H_C = 50$ Oe and $m_r = 0.07$. The remanent magnetization in the perpendicular direction increases with n , $m_r = 0.75, 0.86, 0.94,$ and 0.90 for $n = 10, 15, 20,$ and 40, respectively, while the coercive field

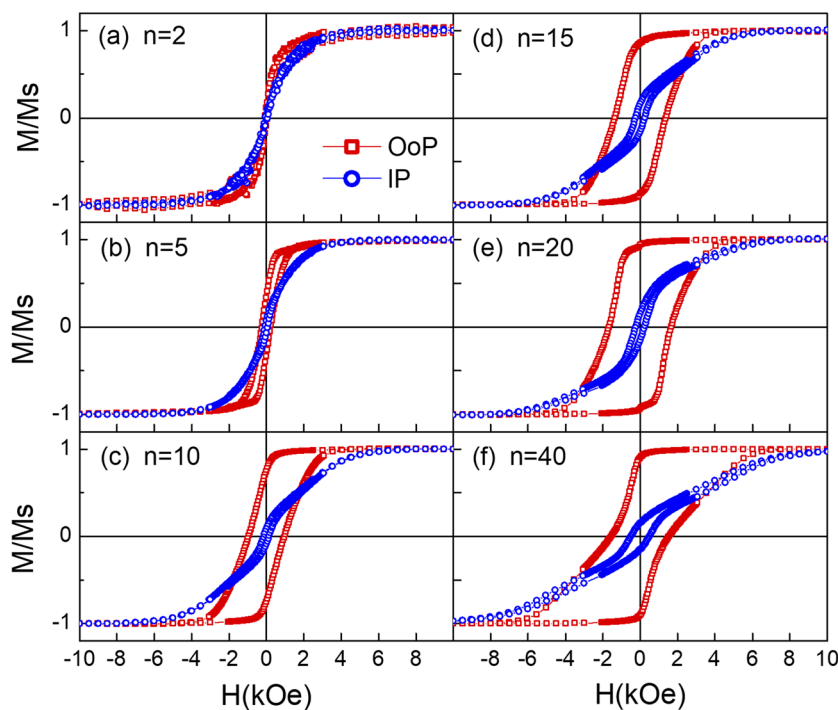


FIG. 1. Normalized magnetization curves for $n = 2, 5, 10, 15, 20,$ and 40. External field applied in-plane (IP) and perpendicular to the sample surface [out-of-plane (OoP)].

progressively grows up to 1600 Oe. These data demonstrate that the OoP direction is the more favorable orientation of the magnetization as n increases, while the IP surface becomes a harder magnetic axis with n . Consequently, the saturation field of IP hysteresis loops gradually evolves from 3500 Oe for $n = 5$ up to 9000 Oe for $n = 40$.

The Co saturation magnetization (M_S^{Co}) was obtained from the absolute value of the magnetic moment of each sample at high fields and the volume of the Co layers. The sample area was digitally measured using the ImageJ open source,³³ and the Co thickness was estimated as the Co-nominal thickness of the multilayer. It is worth mentioning that XMCD measurements show a Pd polarization by the proximity effect of Co atoms; however, the Pd magnetization is almost one order of magnitude smaller than the Co magnetization and is omitted in this calculation.^{10,27} Figure 2 plots the progression of M_S^{Co} with the number of repetitions (blue dots) and the bulk Co magnetization from the literature (red triangle) for comparison. Thicker samples ($n \geq 15$) exhibit the same saturation magnetization as the Co bulk. However, M_S^{Co} decreases for thinner multilayers down to 27% of the pure Co magnetization for $n = 2$. It reveals a neighboring effect at the initial growth of the Co/Pd film.³⁴

The effective anisotropy of each sample was calculated from magnetometry measurements. The magnetic anisotropy energy density is given by the area enclosed between the OoP and IP magnetization curves. In our case, these curves present hysteresis; thus, the averaging curve of the decreasing and increasing branches of the hysteresis loop was previously calculated, and is used to numerically compute the anisotropy energy in the H interval [0 kOe, 10 kOe].¹⁰ The differential area, K_{eff} , is plotted in Fig. 3 for each multilayer. The effective anisotropy monotonously increases with the number of repetitions. Taking this into account, the anisotropy can be phenomenologically separated in a volume contribution that yields in-plane anisotropy (negative) and an interfacial contribution from Co/Pd interfaces (positive) responsible for the perpendicular orientation of the magnetization, a positive value of K_{eff} indicates a preferential direction perpendicular to the sample plane. In our multilayer system, the OoP orientation is energetically more favorable as the number of repetitions increases, improving the perpendicular

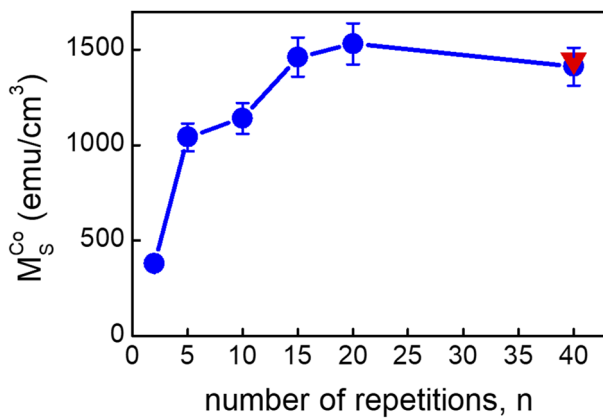


FIG. 2. Magnetic moment of Co/Pd multilayers per Co-volume (blue circles). Bulk Co magnetization at room temperature (red triangle).

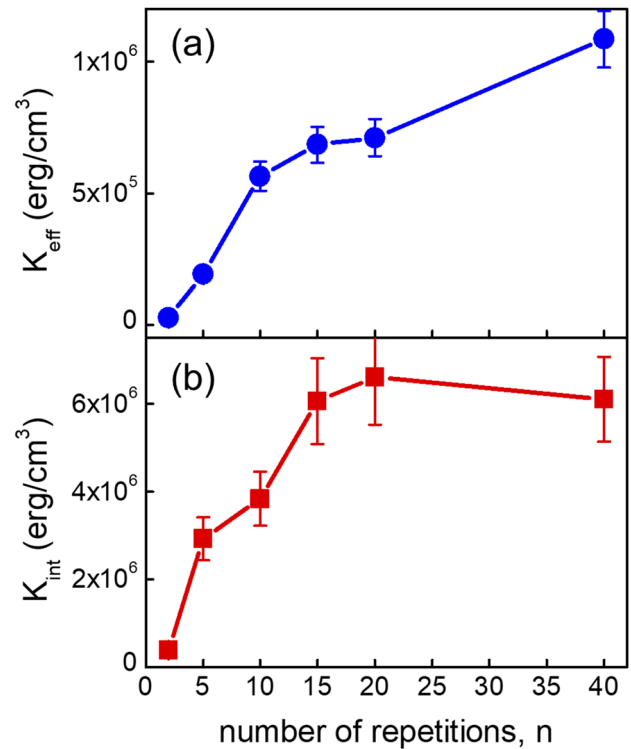


FIG. 3. (a) Effective anisotropy energy of Co/Pd multilayers obtained from the energy difference between OoP and IP magnetization curves (irreversible curves were averaged for integration). Positive values result in PMA (b) Intrinsic anisotropy energy at the Co/Pd interface calculated from $K_{\text{eff}} = K_{\text{int}} + K_{\text{d}}$. The demagnetization energy was estimated as $K_{\text{d}} = -2\pi(M_s^{\text{Co}})^2 \cdot t_{\text{Co}} / (t_{\text{Co}} + t_{\text{Pd}})$.

magnetic anisotropy of the system with n . Contrary to other experimental studies in which a maximum in K_{eff} and M_S^{Co} was observed between 5 and 10 repetitions,^{35,36} our multilayer system holds a constant value of K_{int} and M_S^{Co} for the n range between 15 and 40, and a monotonous increase in K_{eff} with the repetition number. Thus, this system extends the maximum intrinsic parameters in a wide range of thicknesses. This finding allows the design of multilayers and patterned nanoelements with higher magnetic moments keeping a strong PMA.

The main source of the volume anisotropy energy is the demagnetization energy of the film—the magnetocrystalline anisotropy of bulk fcc Co is negligible due to the symmetry of the structure.¹⁰ Therefore, K_{eff} can be written as

$$K_{\text{eff}} = K_{\text{int}} + K_{\text{d}},$$

where K_{int} accounts for the intrinsic anisotropy from Co/Pd interfaces and K_{d} is the demagnetization energy density, which can be estimated as

$$K_{\text{d}} = -2\pi(M_s^{\text{Co}})^2 \cdot t_{\text{Co}} / (t_{\text{Co}} + t_{\text{Pd}}).$$

Considering that Pd has a much lower magnetic moment than Co, K_{d} was calculated for each multilayer from the Co saturation magnetization values of Fig. 2 and the nominal Co and Pd layer thicknesses (t_{Co} , t_{Pd}).

The intrinsic anisotropy was calculated as the difference between the experimentally measured K_{eff} and the estimated K_d , and plotted in Fig. 3(b). K_{int} shows a fast growth from $n = 2$ to 15 and keeps a constant value for $n \geq 15$, following a similar trend to the Co saturation magnetization.

In order to explore the microscopic origin and evolution of the intrinsic anisotropy with the number of Co/Pd repetitions, XMCD spectra were obtained at room temperature for $n = 2, 5, 10, 20$, and 40.

Effective spin and orbital magnetic moments were specifically obtained for Co from the spectra by applying the XMCD sum rules,^{37,38} following the procedure described by Chen *et al.*³⁹ and considering 2.43 holes per Co atom.⁴⁰ Figure 4(a) presents the evolution of the perpendicular and in-plane components of the orbital magnetic moment with the number of repetitions, m_{orb}^{\perp} and $m_{\text{orb}}^{\parallel}$, respectively. Both components follow the same trend; a low magnetic moment in very thin multilayers that increases with n and saturates for $n \geq 10$. Moreover, both components have a rather close

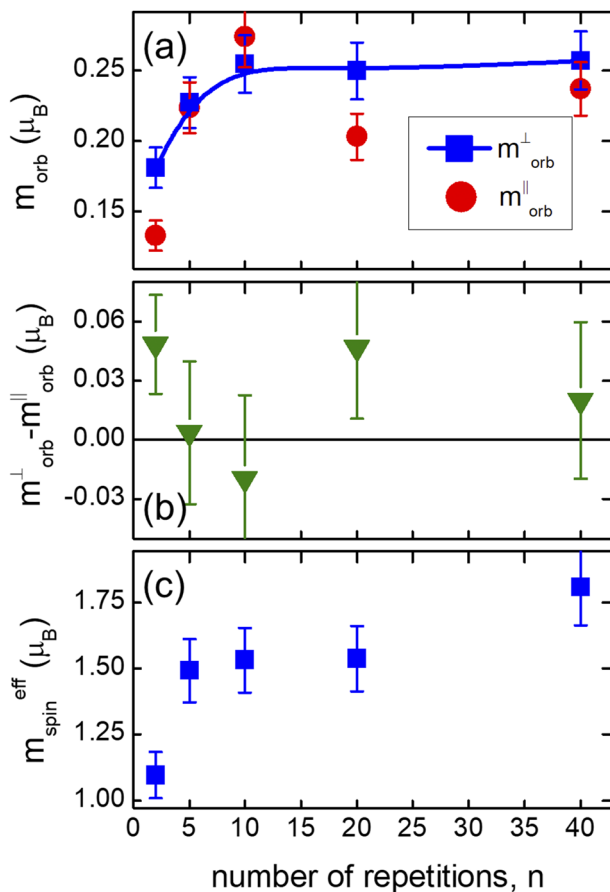


FIG. 4. (a) Orbital magnetic moment per Co atom perpendicular and parallel to the sample surface (solid line is a guide to the eye). (b) Anisotropy of the orbital magnetic moment. (c) Effective spin magnetic moment (isotropic for perpendicular and parallel measurements). Magnetic moments in Bohr magneton units were calculated considering 2.43 holes per Co atom.⁴⁰

magnitude; thus, the difference $m_{\text{orb}}^{\perp} - m_{\text{orb}}^{\parallel}$ that accounts for the anisotropy of the orbital magnetic moment does not show a clear trend with n within the accuracy of the experiment, Fig. 4(b). The $m_{\text{spin}}^{\text{eff}}$ obtained from the XMCD spectra is plotted in Fig. 4(c). It shows a similar n -dependence as that observed for the orbital momentum, a low spin moment for $n = 2$, and a saturated value for $n \geq 10$. Thus, the enhancement of both $m_{\text{spin}}^{\text{eff}}$ and m_{orb} with the number of Co/Pd repetitions is connected to each other and correlated with the saturation magnetization and the intrinsic anisotropy of the samples.

To gain further insights into the magnetic properties of the Pd/Co multilayers, we investigated the XMCD signal at the Pd $L_{2,3}$ as a function of the number of repetitions for $n = 5, 10, 20$, and 40. The Pd $m_{\text{spin}}^{\text{eff}}$ and m_{orb}^{\perp} were also obtained by employing the XMCD sum rules. In this case, we employed the approach developed by Vogel *et al.*³⁷ The result of the sum rule analysis is reported in Fig. 5. It overall shows a trend for larger Pd orbital and spin moments at high repetitions ($n = 20, 40$), and Pd moments up to 0.25 Bohr magnetons, which are rather close to values previously reported in the literature when taking into account the accuracy of sum rules.³⁷

The macroscopic and microscopic techniques used for the magnetic characterization allow us to establish important correlations between the bulk and atomic magnitudes. There is a clear relationship between the spin magnetic moment per Co atom obtained by circular dichroism [Fig. 4(c)] and the Co magnetization of the sample (Fig. 2). Although the Co spin moment increases up to $n = 10$, while the M_s^{Co} grows up to $n = 15$, it might be a consequence of the volume probed by each technique. Magnetometry measurements collect the full signal of the sample, while the electron yield technique

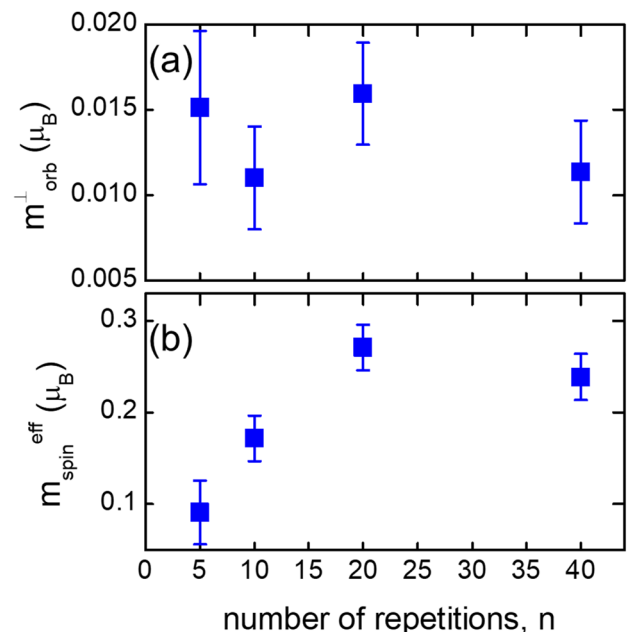


FIG. 5. Magnetic moments per Pd atom at normal incidence calculated employing the XMCD sum rules as a function of the number of repetitions. (a) Orbital magnetic moment. (b) Effective spin magnetic moment.

of XMCD is only sensitive to the outmost planes of the multilayer, ~ 4 nm from the top surface.²⁸ A very low number of repetitions present a low spin moment due to poor atomic coordination of Co atoms at the very first atomic layers, maybe due to the diffusion with the Si substrate. The local environment improves with n , and this improvement is rapidly detected by XMCD probing the last Co/Pd repetitions. However, M_s^{Co} was calculated from the SQUID signal coming from the whole sample, averaging all the Co layers. Consequently, a large number of repetitions is needed to disregard the contribution of the first atomic layers. It must be mentioned that both techniques agree to estimate magnetic quantities equivalent to those of bulk Co. All samples above 15 repetitions possess the same saturation magnetization as the bulk Co magnetization (red triangle in Fig. 2), and within the experimental error, the atomic Co magnetic moment compares to that of the bulk Co, $1.7 \mu_B$ [Fig. 4(c)].

Perpendicular magnetic anisotropy is attributed to a dominant intrinsic anisotropy over the bulk anisotropy. The microscopic origin of this surface anisotropy has been discussed in the last few decades with experimental and theoretical studies. The experimental evidence of a connection between macroscopic measurements and atomic parameters was not always conclusive.^{27,28} In our system, the XMCD analysis demonstrates a direct correlation of the Co-orbital moment [Fig. 4(a)] with the intrinsic anisotropy [Fig. 3(b)]. Both magnitudes increase with the number of repetitions and reach a constant value at $n = 15$ and $n = 10$, respectively. Again, the difference in the number of repetitions at which these magnitudes remain constant can be attributed to the superficial character of the XMCD technique. The saturated value of the Co-orbital moment ($0.25 \mu_B$) is much higher than the orbital moment of pure Co thin films ($0.17 \mu_B$),⁴¹ which demonstrates the enhancement of the orbital moment due to proximity effects at the Co/Pd interface.

The enhancement of the Co-orbital moment was found in both orthogonal directions, perpendicular and parallel to the surface of the sample. Therefore, the anisotropy of the orbital moment [Fig. 4(b)] yields small values that, within the accuracy of the data, do not allow establishing a clear trend of Δm_{orb} with the number of repetitions. In consequence, we can only identify the n -dependence of macroscopic magnitudes—as K_{eff} and K_{int} —with the atomic Co-orbital moment, which is an evidence for the electronic origin of these magnitudes, but not with the anisotropy of the orbital moment per Co atom. However, this result does not discard a microscopic source of the PMA on the orbital magnetic anisotropy. First-principles calculations estimate that such a small $\Delta m_{\text{orb}} < 0.02 \mu_B$ can yield PMA,⁴² and experimental measures marked $\Delta m_{\text{orb}} < 0.03 \mu_B$,⁴³ which is in the order of the error bar in Fig. 4(b). In addition, other energy terms not considered here, as the strain-induced magnetoelastic contribution or dipole interactions in rough sample interfaces, might positively increase the PMA of the multilayer system.^{36,44,45}

The important correlation observed between Co and Pd magnetic moments is worth noting. The increase in the magnitude of the Co moment with the number of repetitions is also reflected in the Pd moment. It is reasonable to expect that a large Co moment drives, via a proximity effect, a large Pd moment, which enhances the Co–Pd coupling at the interface. As a result, one may consider two mechanisms via the Pd magnetization that favor perpendicular anisotropy. On the one hand, the interface coupling and electronic hybridization between Co and Pd states induce a magnetic anisotropy by increasing the spin–orbit interaction perceived by Co moments. On

the other hand, the magnetic coupling increases the magnetoelastic energy between Co and Pd at the interface, which has also been ascribed as a source of PMA.

In conclusion, Co/Pd multilayers deposited on Si substrates exhibit a progressive perpendicular magnetic anisotropy with the number of repetitions. With an increase in n , the PMA becomes monotonously larger while the intrinsic anisotropy saturates at $n = 15$. These macroscopic parameters correlate well with the n -dependence of both spin and orbital Co magnetic moments estimated from XMCD measurements. The modification of the electronic structure at the Co/Pd interface leads to an enhancement of the Co-orbital moment, and a direct relationship between the intrinsic anisotropy and the OoP Co-orbital moment. Within the accuracy of the experimental data, no connection can be established between the PMA and the atomic anisotropy of the Co-orbital moment, which might be smaller than the experimental error bar. On the other hand, an enhancement of the Pd spin moment is found in correlation with that of the Co-spin moment, which might not have been evidenced so far. This increases the magnetic coupling between Co and Pd at the interface and provides mechanisms that might significantly contribute to the origin of PMA.

This work received funding from the MINECO-AEI FIS2016-76058, UE FEDER “Una manera de hacer Europa”; the European Union’s Horizon 2020 research and innovation program under the Marie Skłodowska-Curie Grant No. 734801, and the Basque Country Grant Nos. IT1162-19 and PIBA 2018-11. UPV/EHU authors are thankful for the technical and human support provided by the laser facility, x-ray service, electron microscopy, and magnetic measurement units of SGIker UPV/EHU. We acknowledge the access to BL29 at ALBA synchrotron light facility via official Proposal No. 2015091407. M.V. acknowledges funding via MINECO [Grant No. FIS2016-78591-C3-2-R (AEI/FEDER, UE)]. IMDEA Nanociencia acknowledges the support from the “Severo Ochoa” Program for Centers of Excellence in R&D (MINECO, Grant No. SEV-2016-0686). R.M. acknowledges enlightening discussions with Dr. Arturo Ponce-Pedraza (UTSA) on TEM.

DATA AVAILABILITY

Part of the data were generated at the ALBA synchrotron large scale facility. The data that support the findings of this study are available from the corresponding author upon reasonable request.

REFERENCES

- 1 S. Parkin, X. Jiang, C. Kaiser, A. Panchula, K. Roche, and M. Samant, *Proc. IEEE* **91**, 661 (2003).
- 2 A. V. Khvalkovskiy, D. Apalkov, S. Watts, R. Chepulskii, R. S. Beach, A. Ong, X. Tang, A. Driskill-Smith, W. H. Butler, P. B. Visscher, D. Lottis, E. Chen, V. Nikitin, and M. Krounbi, *J. Phys. D: Appl. Phys.* **46**, 074001 (2013).
- 3 Y. C. Lau, H. Kurt, and J. M. D. Coey, *APL Mater.* **1**, 022104 (2013).
- 4 W. Zhang and K. M. Krishnan, *Mater. Sci. Eng. R. Rep.* **105**, 1 (2016).
- 5 F. Hellman, A. Hoffmann, Y. Tserkovnyak, G. S. D. Beach, E. E. Fullerton, C. Leighton, A. H. MacDonald, D. C. Ralph, D. A. Arena, H. A. Dürr, P. Fischer, J. Grollier, J. P. Heremans, T. Jungwirth, A. V. Kimel, B. Koopmans, I. N. Krivorotov, S. J. May, A. K. Petford-Long, J. M. Rondinelli, N. Samarth, I. K. Schuller, A. N. Slavin, M. D. Stiles, O. Tchernyshyov, A. Thiaville, and B. L. Zink, *Rev. Mod. Phys.* **89**, 025006 (2017).

- ⁶A. Soumyanarayanan, M. Raju, A. L. Gonzalez Oyarce, A. K. C. Tan, M.-Y. Im, A. P. Petrović, P. Ho, K. H. Khoo, M. Tran, C. K. Gan, F. Ernult, and C. Panagopoulos, *Nat. Mater.* **16**, 898 (2017).
- ⁷M. Mann and G. S. D. Beach, *APL Mater.* **5**, 106104 (2017).
- ⁸S.-h. C. Baek, V. P. Amin, Y.-W. Oh, G. Go, S.-J. Lee, G.-H. Lee, K.-J. Kim, M. D. Stiles, B.-G. Park, and K.-J. Lee, *Nat. Mater.* **17**, 509 (2018).
- ⁹H.-Y. Lee, S. Kim, J.-Y. Park, Y.-W. Oh, S.-Y. Park, W. Ham, Y. Kotani, T. Nakamura, M. Suzuki, T. Ono, K.-J. Lee, and B.-G. Park, *APL Mater.* **7**, 031110 (2019).
- ¹⁰M. T. Johnson, P. J. H. Bloemen, F. J. A. d. Broeder, and J. J. d. Vries, *Rep. Prog. Phys.* **59**, 1409 (1996).
- ¹¹A. Hierro-Rodríguez, M. Vélez, R. Morales, N. Soriano, G. Rodríguez-Rodríguez, L. M. Álvarez-Prado, J. I. Martín, and J. M. Alameda, *Phys. Rev. B* **88**, 174411 (2013).
- ¹²C. Blanco-Roldán, C. Quirós, A. Sorrentino, A. Hierro-Rodríguez, L. M. Álvarez-Prado, R. Valcárcel, M. Duch, N. Torras, J. Esteve, J. I. Martín, M. Vélez, J. M. Alameda, E. Pereiro, and S. Ferrer, *Nat. Commun.* **6**, 8196 (2015).
- ¹³Y.-W. Oh, S.-h. Chris Baek, Y. M. Kim, H. Y. Lee, K.-D. Lee, C.-G. Yang, E.-S. Park, K.-S. Lee, K.-W. Kim, G. Go, J.-R. Jeong, B.-C. Min, H.-W. Lee, K.-J. Lee, and B.-G. Park, *Nat. Nanotechnol.* **11**, 878 (2016).
- ¹⁴X. Qiu, Z. Shi, W. Fan, S. Zhou, and H. Yang, *Adv. Mater.* **30**, 1705699 (2018).
- ¹⁵T. Nozaki, T. Yamamoto, S. Tamaru, H. Kubota, A. Fukushima, Y. Suzuki, and S. Yuasa, *APL Mater.* **6**, 026101 (2018).
- ¹⁶I. K. Schuller, R. Morales, X. Batlle, U. Nowak, and G. Güntherodt, *J. Magn. Magn. Mater.* **416**, 2 (2016).
- ¹⁷C. Quirós, S. M. Valvidares, O. Robach, and S. Ferrer, *J. Phys.: Condens. Matter* **17**, 5551 (2005).
- ¹⁸S. M. Valvidares, J. Dorantes-Dávila, H. Isern, S. Ferrer, and G. M. Pastor, *Phys. Rev. B* **81**, 024415 (2010).
- ¹⁹O. Robach, C. Quiros, P. Steadman, K. F. Peters, E. Lundgren, J. Alvarez, H. Isern, and S. Ferrer, *Phys. Rev. B* **65**, 054423 (2002).
- ²⁰S. Ikeda, K. Miura, H. Yamamoto, K. Mizunuma, H. D. Gan, M. Endo, S. Kanai, J. Hayakawa, F. Matsukura, and H. Ohno, *Nat. Mater.* **9**, 721 (2010).
- ²¹B. J. Kirby, J. E. Davies, K. Liu, S. M. Watson, G. T. Zimanyi, R. D. Shull, P. A. Kienzle, and J. A. Borchers, *Phys. Rev. B* **81**, 100405(R) (2010).
- ²²L. Tryputen, F. Guo, F. Liu, T. N. A. Nguyen, M. S. Mohseni, S. Chung, Y. Fang, J. Åkerman, R. D. McMichael, and C. A. Ross, *Phys. Rev. B* **91**, 014407 (2015).
- ²³A. F. Franco, C. Gonzalez-Fuentes, R. Morales, C. A. Ross, R. Dumas, J. Åkerman, and C. Garcia, *Phys. Rev. B* **94**, 064431 (2016).
- ²⁴D. Navas, N. Soriano, F. Béron, C. T. Sousa, K. R. Pirota, J. Torrejon, C. Redondo, R. Morales, and C. A. Ross, *Phys. Rev. B* **96**, 180403(R) (2017).
- ²⁵T.-Y. Chen, Y. Ou, T.-Y. Tsai, R. A. Buhrman, and C.-F. Pai, *APL Mater.* **6**, 121101 (2018).
- ²⁶J. M. Alameda, D. Givord, R. Lemaire, and Q. Lu, *J. Appl. Phys.* **52**, 2079 (1981).
- ²⁷D. Weller, Y. Wu, J. Stöhr, M. G. Samant, B. D. Hermsmeier, and C. Chappert, *Phys. Rev. B* **49**, 12888 (1994).
- ²⁸J. Stöhr, *J. Magn. Magn. Mater.* **200**, 470 (1999).
- ²⁹O. Robach, C. Quirós, H. Isérn, P. Steadman, K. F. Peters, and S. Ferrer, *Phys. Rev. B* **67**, 220405(R) (2003).
- ³⁰C. Du, H. Wang, F. Yang, and P. C. Hammel, *Phys. Rev. Appl.* **1**, 044004 (2014).
- ³¹A. Gomez, D. A. Gilbert, E. M. Gonzalez, K. Liu, and J. L. Vicent, *Appl. Phys. Lett.* **102**, 052601 (2013).
- ³²J. Del Valle, A. Gomez, E. M. Gonzalez, M. R. Osorio, D. Granados, and J. L. Vicent, *Sci. Rep.* **5**, 15210 (2015).
- ³³C. A. Schneider, W. S. Rasband, and K. W. Eliceiri, *Nat. Methods* **9**, 671 (2012).
- ³⁴F. Aguilera-Granja, A. Vega, J. Rogan, X. Andrade, and G. García, *Phys. Rev. B* **74**, 224405 (2006).
- ³⁵C. J. Tatnalp, D. E. Joyce, P. J. Grundy, J. Schille, and G. Van Der Laan, *J. Magn. Magn. Mater.* **177-181**, 1181 (1998).
- ³⁶Y. Liu, J. Qiu, S. T. Lim, S. L. Toh, Z. Zhu, G. Han, and K. Zhu, *Appl. Phys. Express* **10**, 013005 (2017).
- ³⁷J. Vogel, A. Fontaine, V. Cros, F. Petroff, J.-P. Kappler, G. Krill, A. Rogalev, and J. Goulon, *J. Magn. Magn. Mater.* **165**, 96 (1997).
- ³⁸B. T. Thole, P. Carra, F. Sette, and G. van der Laan, *Phys. Rev. Lett.* **68**, 1943 (1992).
- ³⁹C. T. Chen, Y. U. Idzerda, H.-J. Lin, N. V. Smith, G. Meigs, E. Chaban, G. H. Ho, E. Pellegrin, and F. Sette, *Phys. Rev. Lett.* **75**, 152 (1995).
- ⁴⁰R. Cid, J. M. Alameda, S. M. Valvidares, J. C. Cezar, P. Bencok, N. B. Brookes, and J. Díaz, *Phys. Rev. B* **95**, 224402 (2017).
- ⁴¹Y. Wu, J. Stöhr, B. D. Hermsmeier, M. G. Samant, and D. Weller, *Phys. Rev. Lett.* **69**, 2307 (1992).
- ⁴²Y. Miura, M. Tsujikawa, and M. Shirai, *J. Appl. Phys.* **113**, 233908 (2013).
- ⁴³J. Okabayashi, Y. Miura, and H. Munekata, *Sci. Rep.* **8**, 8303 (2018).
- ⁴⁴A. Braun, *Physica B* **373**, 346 (2006).
- ⁴⁵S. Mohanan and U. Herr, *J. Appl. Phys.* **102**, 093903 (2007).